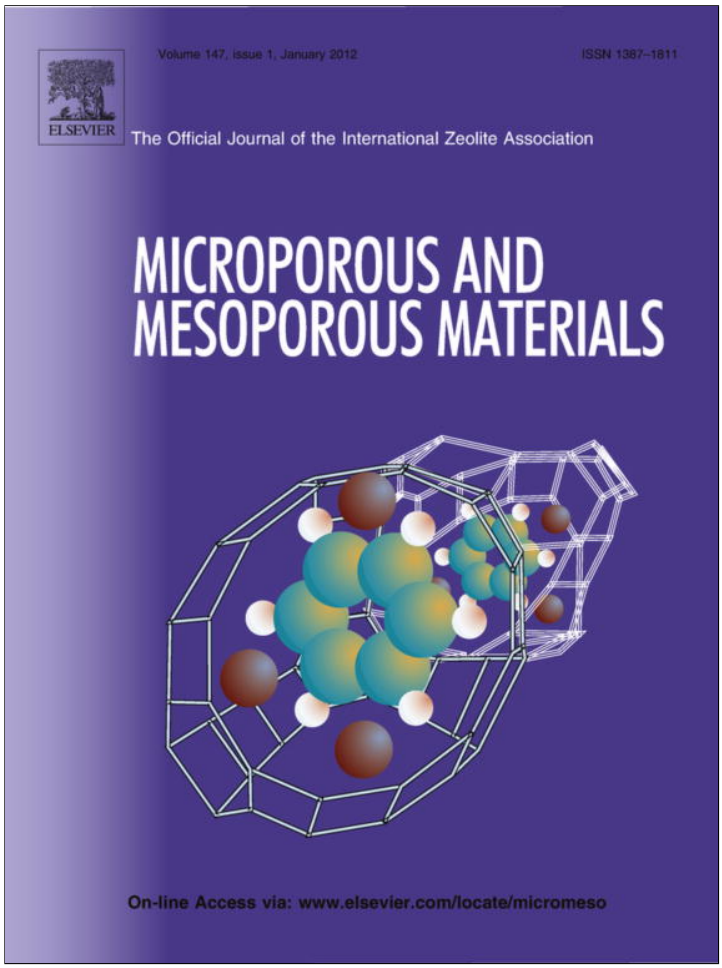

(This is a sample cover image for this issue. The actual cover is not yet available at this time.)

Microporous and Mesoporous Materials 156 (2012) 138–144

Contents lists available at SciVerse ScienceDirect

Microporous and Mesoporous Materials

journal homepage: www.elsevier.com/locate/micromeso

Adsorption of the antibiotic minocycline on cerium(IV) oxide: Effect of pH, ionic strength and temperature

Maximiliano Brigante *, Pablo C. Schulz

INQUISUR, Departamento de Química, Universidad Nacional del Sur, Av. Alem 1253, 8000 Bahía Blanca, Argentina

ARTICLE INFO

Article history:
Received 14 December 2011
Received in revised form 6 February 2012
Accepted 18 February 2012
Available online 28 February 2012

Keywords:
Ceria
Solid–water interface
Minocycline adsorption
Electrostatic interactions
H-bonding

ABSTRACT

Adsorption of the antibiotic minocycline (MC) on cerium(IV) oxide, CeO_2, has been studied in batch experiments by performing adsorption isotherms/kinetics under different conditions of pH, supporting electrolyte concentration, and temperature. CeO_2 was composed by nanoparticles whose grain size was around 9 nm. The adsorption of MC on the studied material is strongly dependent on pH, increasing as pH decreases. The adsorption mechanism, controlled by diffusion processes, is strongly related to electrostatic attractions and H-bond formations mainly between dimethylamino, amide, carbonylic and phenolic groups of the antibiotic and the functional groups of CeO_2 nanoparticles. On the other hand, the adsorption capacity at constant pH increases as ionic strength decreases and as temperature increases. The analysis of thermodynamic parameters suggests that the adsorption on CeO_2 is endothermic and not spontaneous in nature. Ceria nanoparticles might act as an alternative adsorbent for pollution control.

1. Introduction

Pharmaceutical antibiotics are used extensively worldwide in human therapy and farming industry. In the United States alone, the annual antibiotic production was estimated to be 227 million kilograms in 2000 [1]. The antibiotics administered are often poorly metabolized and absorbed by humans and animals and, therefore, tend to enter the aquatic environment [2–4]. Exposure to residues of antibiotics and their transformed products might cause a variety of adverse effects, including acute and chronic toxicity and microorganisms antibiotic resistance [5,6]. However, the removal of antibiotics by conventional water treatment technologies is incomplete [7,8]. Hence, there is an increasing demand for developing more effective treatment technologies to remove pharmaceutical antibiotics from water.

Removal of antibiotics and other anthropogenic compounds by adsorption is considered the major cause of pollutant deactivation and it is important from the point of view of both inhibiting their toxic properties and restricting their transport into water systems. A widely variety of solids such as clays, metal oxides and activated carbon have been used for those purposes. Some of them are good adsorbents in certain experimental conditions but have little or no capacity to adsorb in natural conditions [9], which facilitates the antibiotic leaching into groundwaters. On the contrary, other solids have high affinity for contaminants, protecting them in the adsorbed state from the attack of microorganisms and preventing its degradation [10]. Due to its strong adsorption affinity and relatively low cost, activated carbon has been commonly used as an effective adsorbent for many antibiotics. However, this material has several disadvantages such as (a) it is inactive towards hydrophilic and/or electrical-charged molecules, (b) it predominantly consists of micropores (<2 nm in size) with irregular-shape, closed pore structures, where the adsorption of bulky organic chemicals might be greatly impeded by the size exclusion effect, (c) its working capacity decreases in the presence of natural organic matter, and (d) its regeneration is questionable [11,12]. Recently, we have reported the use of a mesoporous titania–silica material as a very effective solid for removal the antibiotic tetracycline due to its both high adsorptive and catalytic capacities [13].

In this work we have used cerium(IV) oxide or ceria, CeO_2. This material is a cubic fluorite-type oxide, and is considered as the most important of rare-earth oxide, due to extraordinary thermal and chemical stability, which makes the system promising for many application patents [14]. The high level of interest is due to important industrial applications such as solid oxide fuel cells, insulators, high refractive index materials, UV filters, polishing materials, gas sensors, high-temperature oxidation resistance, free-radical scavengers, etc. [14–19]. The use of CeO_2 as catalysts and adsorbents have been also reported [20]. It can maintain excellent adsorption capacity at temperatures as high as 800 °C under some specific conditions [21,22], and over a wide pH range [23,24]. The presence of common anions such as nitrate, chloride, sulfate, and carbonate in aqueous solution has no significant impact on its adsorption ability [23,24]. CeO_2 can be commercially obtained or it can be synthesized in a laboratory with a mesoporous structure by using cerium(III

* Corresponding author. Tel.: +54 291 4595101x3523.
E-mail address: brigante@uns.edu.ar (M. Brigante).

1387-1811/$ - see front matter © 2012 Elsevier Inc. All rights reserved.
doi:10.1016/j.micromeso.2012.02.033

and/or IV) inorganic salts as ceria precursors and ionic and/or non-ionic surfactants as templates [14].

The aim of this article is thus to present a study of adsorption of the antibiotic minocycline on mesoporous CeO_2, which was synthesized in our laboratory by using cerium(IV) sulfate as ceria precursor and cetyltrimethylammonium tosylate as template. The data obtained at a variety of pH, ionic strengths, and temperatures are used to gain insights into the mechanisms that govern the adsorption process and into the factors that promote or prevent adsorption. Minocycline (MC) is an antibiotic from tetracycline's family that exhibit broad-spectrum antimicrobial activities against a variety of disease producing bacteria. The maximum permissible concentration of MC (and others tetracyclines) in aqueous solutions for industrial and pharmacy wastewaters is very low (1 μg L^{-1}) although concentrations of 15 μg L^{-1} MC in wastewater effluents have been reported [25]. It bears different charges on different sites depending on solution pH as shown in Fig. 1. The fully protonated species of MC exists at low pH values (MCH_4^{2+}). As the pH increases, the first deprotonation step (p*K*a = 2.8) occurs at the hydroxyl group on C3 leading to the formation of a species with one positive charge (MCH_3^{+}). The second deprotonation step (p*K*a = 5.0) takes place in the aromatic amino group generating a zwitterionic species ($MCH_2^{\pm}$. The third deprotonation (p*K*a = 7.8) involves the O10–O12 ketophenolic hydroxyl group giving rise to a species with negative charge (MCH^{-}). Finally, the fourth deprotonation (p*K*a = 9.5) involves the dimethylamino group giving rise to a species with two negative charges (MC^{2-}) [26,27].

2. Materials and methods

2.1. Chemicals

Cetyltrimethylammonium *p*-toluene sulfonate or tosylate (CTAT, MW = 455.7 g mol^{-1}) was obtained from Aldrich. Cerium(IV) sulfate were purchased from BDH Reagents & Chemicals. NaOH, KCl, KNO_3, HNO_3. HCl, sodium acetate, acetic acid, sodium carbonate, sodium hydrogen carbonate, disodium phosphate anhydrous, and monosodium phosphate anhydrous were obtained from Anedra. Minocycline hydrochloride was purchased from PARAFARM, and its purity (99%) was confirmed by X-ray diffraction (XRD) and FT-IR spectroscopy. All chemicals were of analytical grade and used as received. Doubly distilled water was used for the preparation of solutions.

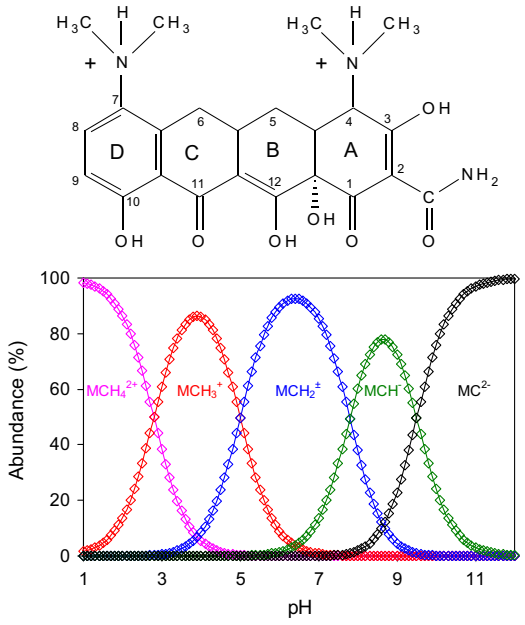

Fig. 1. Molecular structure of fully protonated minocycline and its speciation under different pH values in aqueous solution.

2.2. Synthesis and characterization of CeO_2

Ceria was obtained as follows: 40 mL of CTAT solution was prepared by adding 0.261 g of the surfactant to water. Then, 20 mL of NaOH 1.375 M was added to the surfactant solution under vigorous stirring. To obtain the mesoporous material 1 g cerium(IV) sulfate was added 15 min after the addition of the NaOH solution. The final molar gel composition of the mixture was: 1 $Ce(SO_4)_2$:0.19 CTAT:9.14 NaOH:1107 H_2O. The resulting material was stirred for 30 min at 500 rpm and then left for 24 h at room temperature. Then, it was filtered and washed with distilled water and left to dry at room temperature. Finally, it was calcined in an air flux by increasing the temperature from room temperature to 540 °C with a heating rate of 2 °C min^{-1}, and holding for 7 h at 540 °C.

The synthesized CeO_2 was characterized by the techniques usually employed in porous materials, such as scanning and transmission electron microscopy; XRD; FT-IR spectroscopy; electrophoretic mobility measurements; and the N_2-BET method for surface area, pore volume and pore diameter determination. Scanning electron microscopy (SEM) was performed using an EVO 40-XVP microscope. The sample was prepared on graphite stubs and coated with a ca. 300 Å gold layer in a PELCO 91,000 sputter coater. Transmission electron microscopy (TEM) was performed using a JEOL 100 CX II transmission electron microscope, operated at 100 kV with magnification of 450,000×. Observations were made in a bright field. The powdered sample was placed on copper supports of 2000 mesh. XRD patterns were collected via a Philips PW 1710 diffractometer with CuKα radiation (λ = 1.5406 Å) and graphite monochromator operated at 45 kV, 30 mA and 25 °C. The isoelectric point (IEP) of CeO_2 was measured with a Zetasizer Nano Series instrument (Malvern Instruments Ltd.) at room temperature. Stock CeO_2 suspensions containing 0.1 g L^{-1} of solid in 10^{-2} M KNO_3 were used for those purposes. The pH of the suspensions was then adjusted to the desire value by adding small volumes of HNO_3 or KOH solutions. The N_2 adsorption isotherms at 77.6 K were measured with a Quantachrome Nova 1200e instrument. The sample was degassed at 373 K for 720 min at a pressure of 1×10^{-4} Pa. FT-IR experiments were recorded in a Nicolet FT-IR Nexus 470 spectrophotometer. To avoid co-adsorbed water the sample was dried under vacuum until constant weight was achieved and diluted with KBr powder before the FT-IR spectrum was recorded.

2.3. Adsorption experiments

Adsorption experiments (in darkness to avoid photodegradation) were obtained with a batch equilibration procedure using 15 mL polypropylene centrifuge tubes covered with polypropylene caps immersed in a thermostatic shaker bath. Before starting the experiment, a stock MC solution (5×10^{-4} M) was prepared by adding the corresponding solid to pH buffer solutions. The pHs used in these studies were 4.4, 7.0, and 9.5 by using 0.1 M acetate/acetic acid, $HPO_4^{-2}/H_2PO_4^{-1}$, and CO_3^{-2}/HCO_3^{-1} buffer solutions, respectively. Fifty milligrams of mesoporous material were introduced into the tubes and mixed with varying quantities of MC and KCl (used as supporting electrolyte) solutions. The range of initial MC concentration was 5–400 μM, and the final volume was 8 mL. The stirring rate was kept constant at 90 rpm. At different reaction times, the particles were separated from the supernatant by centrifugation at 4000 rpm during 2 min and the supernatant was immediately analysed to quantify the concentration of

adsorbed MC. After the quantification (see below), that took around 30 s, the supernatant was reintroduced into the tube. This procedure (separation, quantification of MC and reintroduction of the supernatant into the reaction tube) was repeated during several hours in order to achieve complete adsorption of the antibiotic or to gather enough data points. The last data point obtained of these experiments was assumed as equilibrium concentration of MC in the supernatant. Adsorbed MC was calculated from the difference between the initial MC concentration and the concentration of the antibiotic that remained in the supernatant solution. In most experiments no supporting electrolyte was used and the working temperature was 25 °C (except when effects of ionic strength and temperature were investigated).

Quantification of MC was performed by UV–vis spectroscopy at 354 nm for pH 4.4, at 345 nm for pH 7, and at 382 nm for pH 9.5 using an Agilent 8453 UV–vis diode array spectrophotometer equipped with a Hellma 1 cm quartz cell. This is due to the shifting of the maximum absorption band of MC as pH varies. The supernatant of the withdrawn aliquot was placed into the cell and the spectrum was recorded in the 200–900 nm wavelength range. Calibration curves at the working pH were also conducted with several MC solutions having concentrations that ranged between 5×10^{-6} and 1×10^{-3} M. Very good linearity was found in all cases ($r^2 > 0.998$).

The adsorption isotherms were fitted using the Freundlich equation, which was commonly used in the adsorption of antibiotics on several adsorbent systems [8,13]. The linear form of this equation is displayed as follows:

$$\ln\ \mathrm{MC_{ads}} = \ln\ K_F + \frac{1}{n}\ln\ \mathrm{MC_{eq}}, \quad (1)$$

where $\mathrm{MC_{ads}}$ is the adsorbed amount of MC ($\mu\mathrm{mol\,g^{-1}}$); MC_{eq} is the equilibrium concentration of MC in the supernatant (μM); K_F is the Freundlich constant; and $1/n$ is the adsorption intensity. From the linearized form of Eq. (1), K_F, $1/n$, and the correlation coefficient, r^2, can be calculated.

The adsorption kinetic is traditionally described following the expressions of the pseudo-first and the pseudo-second order equations originally given by Lagergren, which are special cases for the general Langmuir rate equation [28]. However, these models cannot give interaction mechanisms, so another model to test antibiotic adsorption on the studied materials was also used. A pore diffusion model, described by Eq. (2), was used here and in most solid/solution interaction studies [13,29]:

$$\ln\ q_t = k_{diff}\ t^{-1/2} + I, \quad (2)$$

where k_{diff} is the pore diffusion rate constant ($\mu\mathrm{mol\,g^{-1}\,min^{-1/2}}$) and I is the intercept ($\mu\mathrm{mol\,g^{-1}}$). If the adsorption mechanism follows the pore diffusion process a plot of $\ln\ q_t$ versus $t^{-1/2}$ should be a straight line with a slope k_{diff} and intercept I.

3. Results and discussion

3.1. Characterization of CeO_2

Fig. 2 shows the electronic micrographs of synthesized sample. According to the SEM image (Fig. 2a), CeO_2 shows randomly shaped aggregates of variable sizes, which is probably due to a faster condensation of ceria during calcination, and these do not provide a clear morphology. The aggregates are formed by nanoparticles whose average diameter is around 9 nm (Fig. 2b), which is in agreement with those reported in literature [30]. Fig. 2b also shows that the nanoparticles are nearly spherical, but have slight faceting indicating the possibility that different

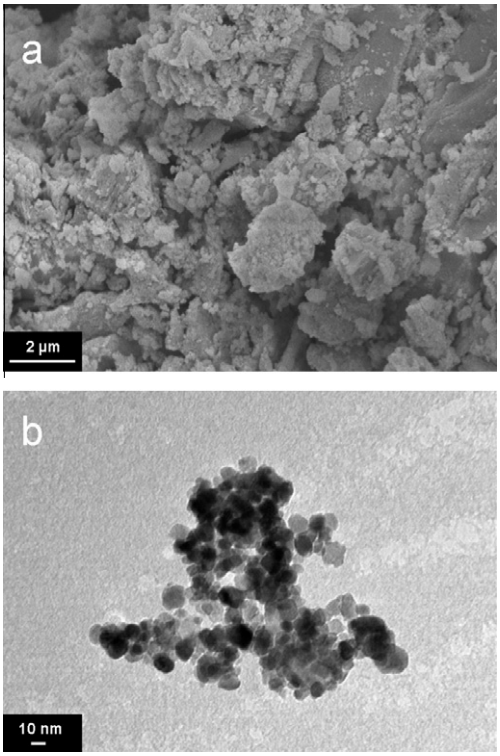

Fig. 2. Electron micrographs of synthesized CeO_2: (a) SEM, 20,000×; and TEM, 450,000×.

crystallographic planes, each with a different atomic density, are interfacing with the aqueous phase [30].

CeO_2 was also characterized by XRD, nitrogen sorption isotherms, electrophoretic mobility and FT-IR spectroscopy and the results are shown in Fig. 3. Ceria shows typical XRD patterns at 2θ = 28.6, 33.2, 47.4, 56.4, 59.1, 69.4, 76.8 and 79.1 (Fig. 3a), which are characteristic of the cubic fluorite structured CeO_2 [30,31]. The strong and sharp diffraction peaks indicate the good crystallization of the samples. No additional peaks in the XRD were observed, revealing the high purity of the prepared ceria nanoparticles. In fact, the grain size of CeO_2 nanoparticles, determined from the width at half maximum of the (1 1 1) peak according to the Scherrer formula [32], is 8.7 nm, which is consistent with the TEM studies. Nitrogen sorption isotherms of CeO_2 are presented in Fig. 3b, which exhibits a type IV isotherm with a H3 hysteresis loop that is characteristic of mesoporous materials [31]. The BET specific surface area and the pore volume are calculated to be 33.52 $\mathrm{m^2\,g^{-1}}$ and 0.06 $\mathrm{cm^3\,g^{-1}}$, respectively. The BJH pore size distribution (inset in Fig. 3b) shows an irregular distribution of the pores in the material. In the range of 1.50–60.00 nm, there are two peaks at 2.02 and 12.92 nm. This irregularity suggests the co-existence of pores with different sizes, which were probably formed by the stacking of CeO_2 particles [33]. Fig. 3c shows the variation of the potential zeta of the studied CeO_2 as a function of the pH. Ceria nanoparticles has an isoelectric point (IEP) of 4, which values are closed with the results reported by Patil et al. [34] and recently by Goharshadi et al. [31] on the synthesis of CeO_2 nanoparticles obtained by microemulsion and microwave methods, respectively. Moreover, Patil et al. [34] reported that the IEP of CeO_2 depends on both the synthesis method and the chemicals involved in the synthesis process. In fact, the use of NH_4OH for the synthesis of CeO_2 by microemulsion process led a material with an IEP of 4.5 whereas the ceria nanoparticles treated with a HCl solution in the last step during hydrothermal synthesis process led a material with an IEP of 9.5. Fig. 3d shows the FT-IR spectrum

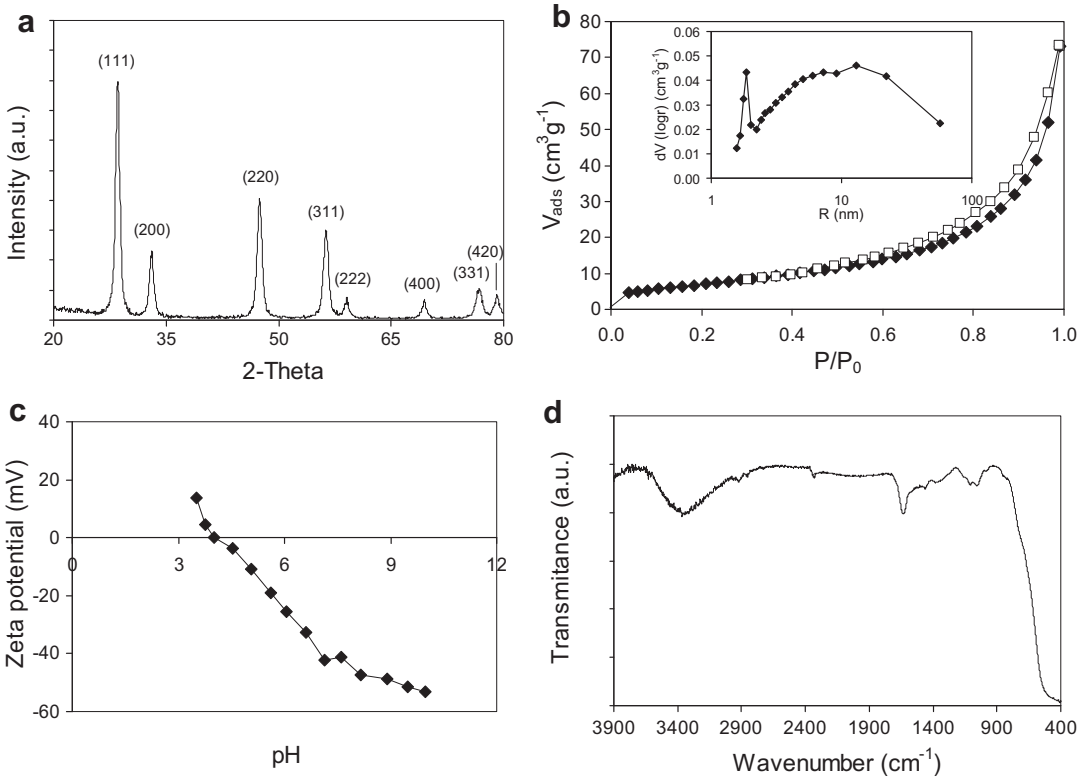

Fig. 3. Characterization of studied sample by: (a) XRD; (b) N_2 adsorption (solid symbols)–desorption (open symbols) isotherms, where the inset shows the pore radius distribution; (c) electrophoretic mobility measurements as a function of pH in a 10^{-3} M KNO_3 solution; and (d) infrared spectroscopy.

of CeO_2. The most important features of this material are a broad band centered at 3395 cm^{-1} associated to physically adsorbed water, a peak located at around 1640 cm^{-1} due to the bending vibration of associated water, and a peak centered at 447 cm^{-1} which is attributed to Ce–O stretching, [35,36]. The vibration peaks located between 980 and 1400 cm^{-1} are similar to that of commercial ceria powders and those reported by Li et al. [37] on the synthesis of 3D flowerlike CeO_2 microspheres.

3.2. MC adsorption studies

Adsorption kinetics of MC on CeO_2 as a function of pH were shown in Fig. 4. The adsorption is very fast between $t = 0$ and 5 min. It is so fast that no data point could be measured in this period with our experimental set up. At $t > 5$ min the adsorption takes place at a much slower and measurable rate. Although adsorption seems to reach completion at around 180 min, some long-term kinetic experiments revealed that adsorption continues after several days, but very slowly. Fig. 4 also shows that the adsorption on both adsorbents is strongly dependent on the pH. It is relatively high at low pH and decreases significantly at higher pH values. All data are fitted well to the pore diffusion model with $r^2 > 0.99$. The k_{diff} values at pH 4.4, 7 and 9.5 are 0.183, 0.077 and 0.016 μmol g^{-1} $min^{-1/2}$, respectively. These values are comparable to those reported in a previous paper on the adsorption of tetracycline on TiO_2 nanoparticles and on the binary system TiO_2–SiO_2 at the same experimental conditions [13] suggesting that CeO_2 can act as a good adsorbent for MC kinetically.

The effect of pH can be better observed in the respective adsorption isotherms shown in Fig. 5. As expected, the adsorption is relatively high at pH 4.4 and decreases significantly at pH 7 and 9.5 indicating that the affinity of MC for CeO_2 surface is higher at

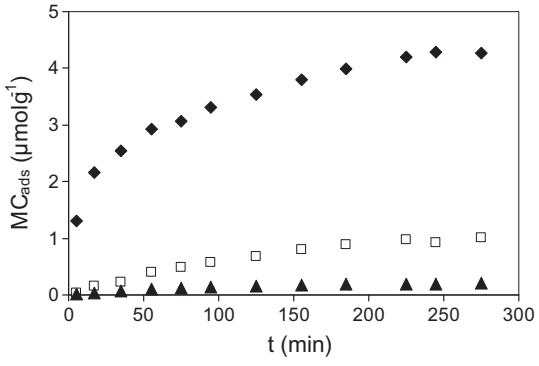

Fig. 4. Effect of pH on the adsorption kinetics of MC on CeO_2 at 25 °C. pH values: solid diamonds, pH 4.4; open squares, pH 7.0; and solid triangles, pH 9.5.

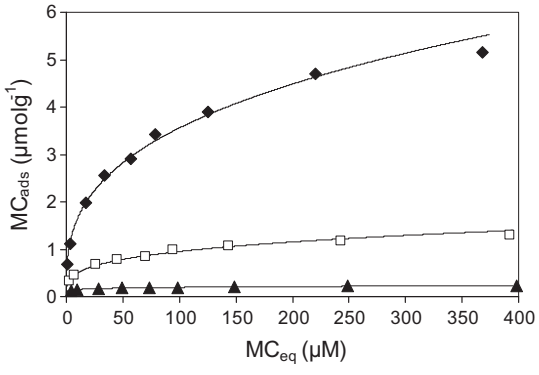

Fig. 5. Effect of pH on the adsorption of MC on CeO_2 at 25 °C. pH values: solid diamonds, pH 4.4; open squares, pH 7.0; and solid triangles, pH 9.5. Lines show predictions of Eq. (1).

low pH. MC adsorption on CeO_2 seems to take place by binding the antibiotic to the ceria, generating surface species MC–CeO_2. The binding between the antibiotic and ceria can be visualized comparing the FT-IR spectra of CeO_2, MC and MC adsorbed on CeO_2 at pH 4.4 such as shown in Fig. 6. MC shows characteristic peaks at 2743 and 2657 cm^{-1} associated to NHR_3^+ group, 1674 and 1520 cm^{-1} assigned to the Amide I and Amide II bands, 1615 and 1582 cm^{-1} assigned to C=O stretching vibration at rings A and C, respectively, 1456 cm^{-1} assigned to C–C stretching vibration, 1357 cm^{-1} assigned to $-CH_3$ deformation vibration, 1244 cm^{-1} which is attributed to C–N amine stretching vibration, and 1176 cm^{-1} assigned to the phenolic C–O stretching band [38]. Ceria peaks are observed in the IR spectra of MC–CeO_2, whereas the bands assigned to NHR_3^+ group are not observed. The peaks assigned to the polar groups of the antibiotic are shifted to lower frequencies with respect to bulk MC. Similar results were found for MC–montmorillonite [26]. The obtained results confirm that the NHR_3^+ groups of MC are bound to the ceria surface, mainly due to electrostatic interactions, whereas other polar groups of the molecule could participate in non-electrostatic interactions (e.g. H-bond formations) with the surface.

The effects of ionic strength on the adsorption of MC isotherms on CeO_2 at pH 4.4 and 25 °C are shown in Fig. 7. The adsorption depends on the ionic strength; it decreases as the KCl concentration increases. These results suggest that formation of ionic pairs or outer-sphere complexes is the prevailing adsorption process: the competition between MC (as MCH_3^+, see Fig. 1) and K^+ for negatively charged groups leads to an important decrease in MC adsorption by increasing K^+ concentration. Results resemble those reported by Li et al. [39] and Chang et al. [40] for the adsorption of tetracycline on kaolinite and palygorskite, respectively, where competition between the antibiotic and electrolyte cations was proposed to play a key role.

The effects of temperature on the adsorption of MC on CeO_2 at pH 4.4 are shown in Fig. 8. The adsorption is significantly affected by varying the temperature from 5 to 45 °C, i.e., the adsorption increases as temperature increases. Several reports exist about the effect of temperature in the adsorption behavior of tetracycline-type antibiotics on different adsorbents. Tanis et al. [41] showed that the adsorption of tetracycline on iron oxides-coated quartz increased by increasing temperature suggesting that a chemisorption-like process may play an important role in the tetracycline-adsorbent system. These observations are significantly different from those reported by Turku et al. [42], who reported that the adsorption of this antibiotic on silica decreased by increasing temperature (physical adsorption). Li et al. [39] showed similar results to those reported by Turku et al. [42] in the tetracycline–kaolinite system at pH higher than 7.7 whereas the adsorption was not significantly affected by varying the temperature at pH 6 or lower.

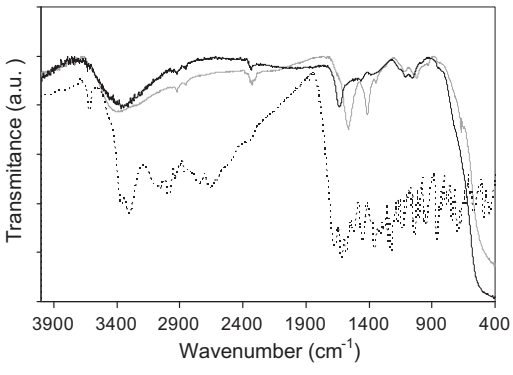

Fig. 6. Infrared spectra of CeO_2(A) (black), MC (dotted), and MC–CeO_2(A) (gray).

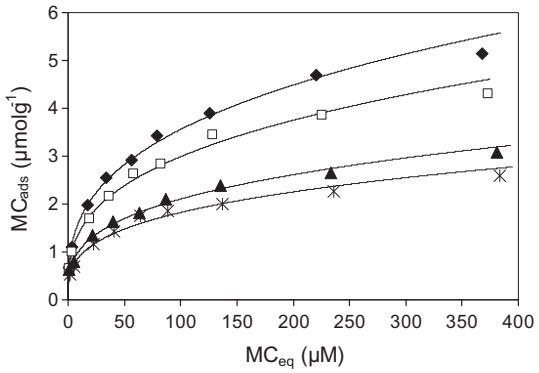

Fig. 7. Effect of ionic strength on the adsorption of MC on CeO_2 at pH 4.4 and 25 °C. KCl concentrations: solid diamonds, 0 M; open squares, 0.003 M; solid triangles, 0.01 M; and stars, 0.1 M. Lines show predictions of Eq. (1).

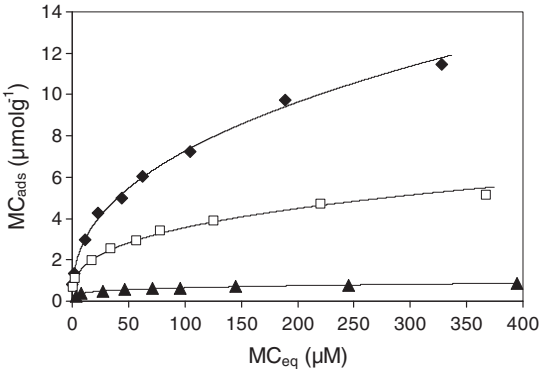

Fig. 8. Effect of temperature on the adsorption of MC on CeO_2 at pH 4.4. Temperatures: solid diamonds, 45 °C; open squares, 25 °C; and solid triangles, 5 °C. Lines show predictions of Eq. (1).

Moreover, a recently paper reported that the adsorption of tetracycline on TiO_2–SiO_2 was not significantly affected by varying the temperature suggesting that the adsorption was strongly dependent on the type of adsorbent [13]. Although the results shown in Fig. 8 seem to agree with those reported by Tanis et al. [41], the strong decrease in adsorption by increasing the ionic strength (Fig. 7) suggests that there is a physical adsorption in our system. In addition, it is known that for adsorption processes controlled by diffusion the rate of the adsorbate molecules across the internal pores of the adsorbent particle increases as temperature increases, owing to the decrease in the viscosity of the solution [43]. This provokes, thus, an increase in adsorption.

From the data showed in Fig. 8 were obtained the thermodynamic parameters of the Gibbs free energy ($\Delta G°$), enthalpy ($\Delta H°$), and the entropy ($\Delta S°$) for the adsorption of MC on the studied material using the following equations:

$$\Delta G^\circ = -RT \ln\left(\frac{MC_s}{MC_{eq}}\right), \quad (3)$$

$$\ln\left(\frac{MC_s}{MC_{eq}}\right) = \frac{\Delta S^\circ}{R} - \frac{\Delta H^\circ}{RT}, \quad (4)$$

where MC_s is the concentration of antibiotic adsorbed (μM), T is the solution temperature in K, and R is the gas constant (8.314 J K^{-1} mol^{-1}). The enthalpy of the MC on CeO_2 is obtained from van't Hoff plots as ln (MC_s/MC_{eq}) versus $1/T$. The thermodynamic parameters are shown in Table 1. Physisorption and chemisorption can be classified, to a certain extent, by the magnitude of

Table 1
Thermodynamic parameters of MC adsorption on CeO_2.

T (°C)	$\Delta G°$ (kJ mol^{-1})	$\Delta H°$ (kJ mol^{-1})	$\Delta S°$ (J K^{-1} mol^{-1})
5	9.87		
25	6.12	45.39	130.67
45	3.77		

Table 2
Best-fit parameters for Eq. (1).

pH	KCl (M)	T (°C)	K_F	n	r^2
9.5	0	25	0.113	8.496	0.989
7.0	0	25	0.264	3.593	0.990
4.4	0	25	0.765	2.995	0.998
4.4	0	5	0.209	3.833	0.994
4.4	0	45	1.107	2.449	0.997
4.4	0.003	25	0.661	3.052	0.996
4.4	0.01	25	0.503	3.216	0.994
4.4	0.1	25	0.446	3.271	0.989

enthalpy change. Bonding strengths of <84 kJ mol^{-1} are typically considered as those of physisorption bonds. Chemisorption bond strengths can be 84–420 kJ mol^{-1} [44]. The $\Delta H°$ value for the adsorption of MC on CeO_2 is positive and 45.39 kJ mol^{-1} implying that the interaction of MC with the solid is an endothermic process, and it confirms that adsorption of the antibiotic onto CeO_2 was driven by a physisorption process. The positive value of $\Delta S°$ (130.67 J K^{-1} mol^{-1}) reflects the affinity of the antibiotic towards solids and may suggest some structural changes in adsorbate (hydration of MC ions) and adsorbent (charged surface upon adsorption) [41]. Finally, the positive value of $\Delta G°$ at the studied temperatures shows that the nature of adsorption on CeO_2 is not spontaneous. However, $\Delta G°$ is less positive with temperature increase showing that the adsorption process can be thermodynamically feasible at higher temperatures.

In Figs. 5, 7 and 8, symbols correspond to data points whereas solid lines correspond to the best-fitting Freundlich isotherms calculated by adjusting the parameters K_F and n. These parameters are listed in Table 2. Even though the formulated model is rather simple, it can fit reasonably well the adsorption of MC, i.e., the goodness-of-fit of Eq. (1) was checked through the r^2 values, which was between 0.989 and 0.997 in all cases. Changes in pH ionic strength and temperature result in important changes in the adsorption isotherm, i.e., K_F decreases as both pH and ionic strength decreases whereas it increases as temperature increases. On the other hand, the Freundlich parameters also show that the adsorption conditions in all cases are favorable ($n > 1$).

4. Conclusions

The results shown in this article reveal that the adsorption of MC on ceria nanoparticles is strongly dependent on pH, increasing as pH decreases. The adsorption mechanism, controlled by diffusion processes, is strongly related to electrostatic attractions and H-bond formations mainly between functional groups of the antibiotic drug and CeO_2. On the other hand, the adsorption capacity at constant pH increases as ionic strength decreases and as temperature increases. The analysis of thermodynamic parameters suggested that the adsorption on CeO_2 is endothermic and not spontaneous in nature.

The obtained results have a significant importance in environmental processes, where the production of synthetic materials can play a key role. Ceria is known to be a very good material for several processes (oxide fuel cells, insulators, high refractive index materials, UV filters, polishing materials, gas sensors, etc.) due to its extraordinary thermal and chemical stability. However CeO_2 can be also used as an excellent adsorbent for several antibiotics, e.g. tetracycline and derivates, due to its mesoporous structure and its high affinity towards hydrophilic molecules (in comparison with e.g. activated carbon). This will not only benefit the deactivation of the mentioned pollutants but also reduce their leaching and transport through groundwaters.

Acknowledgments

This work was financed by SECyT-UNS, CONICET and ANPCYT. The authors thank Olga Pieroni and Leticia Lescano for the FT-IR spectra and X-ray diffractograms, respectively. M. Brigante thanks CONICET for the postdoctoral fellowship.

References

[1] Y.J. Wang, D.A. Jia, R.J. Sun, H.W. Zhu, D.M. Zhou, Environ. Sci. Technol. 42 (2008) 3254–3259.
[2] B. Halling-Sørensen, S. Nors-Nielsen, P.F. Lanzky, F. Ingerslev, H.C. Holten-Lützhøft, S.E. Jørgensen, Chemosphere 36 (1998) 357–393.
[3] R. Hirsch, T.A. Ternes, K. Haberer, K.L. Kratz, Sci. Total Environ. 225 (1999) 109–118.
[4] D.W. Kolpin, E.T. Furlong, M.T. Meyer, E.M. Thurman, S.D. Zaugg, L.B. Barber, H.T. Buxton, Environ. Sci. Technol. 36 (2002) 1202–1211.
[5] A.B.A. Boxall, D.W. Kolpin, B. Halling-Sørensen, J. Tolls, Environ. Sci. Technol. 37 (2003) 286–294.
[6] H. Schmitt, K. Stoob, G. Hamscher, E. Smit, W. Seinen, Microb. Ecol. 51 (2006) 267–276.
[7] T.A. Ternes, A. Joss, H. Siegrist, Environ. Sci. Technol. 38 (2004) 392–399.
[8] L. Ji, F. Liu, Z. Xu, S. Zheng, D. Zhu, Environ. Sci. Technol. 44 (2010) 3116–3122.
[9] Z.Y. Hseu, S.H. Jien, S.F. Cheng, J. Environ. Sci. Health B 38 (2003) 441–449.
[10] L. Scrano, S.A. Bufo, C. Emmelin, P. Meallier, in: E. Lichtfouse, J. Schwarzbauer, D. Robert (Eds.), Environmental Chemistry: Green Chemistry and Pollutants in Ecosystems, Springer, Berlin, cap. 46, 2005, pp. 505–515.
[11] G. Liu, S. Zheng, D. Yin, Z. Xu, J. Fan, F. Jiang, J. Colloid Interface Sci. 302 (2006) 47–53.
[12] N.M. Vieno, H. Harkki, T. Tuhkanen, L. Kronberg, Environ. Sci. Technol. 41 (2007) 5077–5084.
[13] M. Brigante, P.C. Schulz, J. Hazard. Mater. 192 (2011) 1597–1608.
[14] A. Bumajdad, J. Eastoe, A. Mathew, Adv. Colloid Interface Sci. 147 (2009) 56–66.
[15] I.M. Hung, H.P. Wang, W.H. Lai, K.Z. Fung, M.H. Hon, Electrochim. Acta 50 (2004) 745–748.
[16] P. Chen, S. Patil, S. Seal, J.F. McGinnis, Nat. Nanotechnol. 1 (2006) 142–150.
[17] J. Niu, A. Azfer, L.M. Rogers, X. Wang, P.E. Kolattukudy, Cardiovasc. Res. 73 (2007) 549–559.
[18] T.S. Stefanik, H.L. Tuller, J. Eur. Ceram. Soc. 21 (2001) 1967–1970.
[19] M. Yamashita, K. Kameyama, S. Yabe, S. Yoshida, Y. Fujishiro, T. Kawai, T. Sato, J. Mater. Sci. 37 (2002) 683–687.
[20] P. Ji, J. Zhang, F. Chen, M. Anpo, Appl. Catal. B: Environ. 85 (2009) 148–154.
[21] H. Guo, W. Li, H. Wang, J. Zhang, Y. Liu, Y. Zhou, Rare Met. 30 (2011) 58–62.
[22] M. Flytzani-Stephanopoulos, M. Sakbodin, Z. Wang, Science 312 (2006) 1508–1510.
[23] M.J. Haron, F. Ab Rahim, A.H. Abdullah, M.Z. Hussein, A. Kassim, Mater. Sci. Eng. B 149 (2008) 204–208.
[24] Y. Zhang, M. Yang, X. Huang, Chemosphere 51 (2003) 945–952.
[25] A. Pena, M. Paulo, L.J.G. Silva, M. Seifrtová, C.M. Lino, P. Solich, Anal. Bioanal. Chem. 396 (2010) 2929–2936.
[26] M.E. Parolo, M.J. Avena, G. Pettinari, I. Zajonkovsky, J.M. Valles, M.T. Baschini, J. Hazard. Mater. 192 (2011) 1597–1608.
[27] V. Orti, M. Audran, P. Gilbert, G. Bougard, F. Bressolle, J. Chromatogr. B 738 (2000) 357–365.
[28] Y.S. Ho, G. Mc Kay, Process Biochem. 38 (2003) 1047–1061.
[29] C.E. Zubieta, P.V. Messina, C. Luengo, M. Dennehy, O. Pieroni, P.C. Schulz, J. Hazard. Mater. 152 (2008) 765–777.
[30] K.M. Buettner, C.I. Rincio, S.E. Mylon, Colloids Surf. A 366 (2010) 74–79.
[31] E.K. Goharshadi, S. Samiee, P. Nancarrow, J. Colloid Interface Sci. 356 (2011) 473–480.
[32] H.P. Klug, L.E. Alexander, X-ray Diffraction Procedures, Wiley, New York, 1954.
[33] S. Miao, Z. Liu, Z. Miao, B. Han, K. Ding, G. An, Y. Xie, Micropor. Mesopor. Mater. 117 (2009) 386–390.
[34] S. Patil, A. Sandberg, E. Heckert, W. Self, S. Seal, Biomaterials 28 (2007) 4600–4607.
[35] X. Li, F. Chen, X. Lu, C. Ni, Z. Chen, J. Rare Earth 27 (2009) 943–947.
[36] D.E. Zhang, X.M. Ni, H.G. Zheng, X.J. Zhang, J.M. Song, Solid State Sci. 8 (2006) 1290–1293.
[37] J. Li, G. Lu, H. Li, Y. Wang, Y. Guo, Y. Guo, J. Colloid Interface Sci. 360 (2011) 93–99.

[38] C.F. Leypold, M. Reiher, G. Brehm, M.O. Schmitt, S. Schneider, P. Matousek, M. Towrie, Phys. Chem. Chem. Phys. 5 (2003) 1149–1157.
[39] Z. Li, L. Schulz, C. Ackley, N. Fenske, J. Colloid Interface Sci. 351 (2010) 254–260.
[40] P.H. Chang, Z. Li, T.L. Yu, S. Munkhbayer, T.H. Kuo, Y.C. Hung, J.S. Jean, K.H. Lin, J. Hazard. Mater. 165 (2009) 148–155.
[41] E. Tanis, K. Hanna, E. Emmanuel, Colloids Surf. A 327 (2008) 57–63.
[42] I. Turku, T. Sainio, E. Paatero, Environ. Chem. Lett. 5 (2007) 225–228.
[43] M. Doğan, M. Alkan, Ö. Demirbas, Y. Özdemir, C. Özmetin, Chem. Eng. J. 124 (2006) 89–101.
[44] S.D. Faust, O.M. Aly, Adsorption Processes for Water Treatment, Butterworth, 1987.